Self-organized state formation in magnonic vortex crystals

Christian F. Adolff,[1,*] Max Hänze,[1] Andreas Vogel,[1] Markus Weigand,[2] Michael Martens,[1] and Guido Meier[1,3]
[1]*Institut für Angewandte Physik und Zentrum für Mikrostrukturforschung, Universität Hamburg, 20355 Hamburg, Germany*
[2]*Max-Planck-Institut für Intelligente Systeme, Heisenbergstrasse 3, 70569 Stuttgart, Germany*
[3]*The Hamburg Centre for Ultrafast Imaging, Luruper Chaussee 149, 22761 Hamburg, Germany*
(Received 21 June 2013; revised manuscript received 4 December 2013; published 30 December 2013)

We study the polarization-state formation in magnonic vortex crystals via scanning transmission x-ray microscopy. Self-organized state formation is observed by adiabatic reduction of a high-frequency field excitation. The emerging polarization patterns are shown to depend on the frequency of excitation and the strength of the dipolar interaction between the elements. In spite of the complexity of the investigated system, global order caused by local interactions creates polarization states with a high degree of symmetry. A fundamental dipole model and coupled equations of motion are adopted to analytically describe the experimental results. The emerging states can be predicted by a fundamental stability criterion based on the excitability of eigenmodes in the crystal. Micromagnetic simulations give additional insight into the underlying processes.

DOI: 10.1103/PhysRevB.88.224425 PACS number(s): 75.70.Kw, 61.72.−y, 68.37.Yz, 75.50.Bb

Complexity created by periodic arrangement of well-understood building blocks plays an important role in biochemistry, photonics, engineering, and nanoelectrics.[1–4] The periodic arrangement of atoms or molecules as basis determines the physical and sometimes even the chemical properties of crystals.[5,6] In the field of magnetism, wave transmission media that feature an artificial lattice created by a periodically modulated magnetic material are referred to as magnonic crystals.[3] The dynamics of magnonic crystals are described by common concepts of solid state physics, i.e., group velocity, density of states, and band structure.[3,7,8] We investigate so-called magnonic vortex crystals created via rectangular arrangements of magnetic vortices. Vortices form in magnetic nanodisks of suitable geometry, where the magnetization curls in the plane, except in the core region, where it points out of the plane, either up or down, leading to two possible stable states of opposite core polarization p.[9,10] The sense of the in-plane magnetization curling is described via the chirality ($C = \pm 1$). The coupling between the vortices and thereby the crystal properties strongly depend on the polarization of every single vortex in the crystal, leading to many possible crystal states for large magnonic vortex crystals. For instance, the polarization configuration determines the band structure of a magnonic vortex crystal.[11–14] Here we demonstrate experimentally and describe analytically an efficient way to control the vortex-core polarization in a rectangular two-dimensional vortex array of magnetic nanodisks. Using scanning transmission x-ray microscopy we image the magnonic crystal dynamics with time resolution in the subnanosecond regime and simultaneous spatial resolution on the nanometer scale.[15] In the context of memory applications the experiments could provide a method to store multiple bits with a single gateway, a concept that is of increasing importance, e.g., in state-of-the-art solid state disks.[16,17] The experimental results are explained analytically by a fundamental dipole model and a particle model. Experimentally we focus on arrays of 3×3 magnetic vortices. However, the analytical results are applicable to much larger systems. The underlying processes are elucidated by micromagnetic simulations.[18]

We use a magnetic field to excite the gyrotropic mode, which is the fundamental excitation of the vortex ground state.[19] It corresponds to the gyration of the vortex core around its equilibrium position with a frequency in the subgigahertz range.[20] The sense of gyration is determined by the polarization of the vortex core.[19] The gyrotropic mode of isolated vortices can be resonantly excited by a unidirectional magnetic field or electric currents.[21,22] Due to its low frequency in comparison to other excitable modes[23] the gyrotropic mode can be solely addressed. When the amplitude of excitation is increased up to a critical value, the vortices reach a critical velocity and the polarization switches. Thereby the sense of gyration is changed.[21] An isolated vortex switches its polarization randomly once a critical amplitude is overcome.[24] When the amplitude of the driving magnetic field is adiabatically reduced, the vortex relaxes into a random polarization state. For arrays of coupled magnetic vortices we observe self-organized vortex-core state formation. The emerging polarization configuration depends on the frequency of the alternating field. In the following we address the disk arrays as vortex crystals.

We present an experiment where different polarization configurations in a 3×3 vortex crystal are reproducibly obtained by tuning the frequency of a strong excitation. Figure 1 illustrates the experimental setup. The vortices are excited by a harmonic field generated by a high-frequency current applied to a stripline in coplanar waveguide geometry above the array. Arrays of Permalloy ($Ni_{80}Fe_{20}$) disks are prepared with the flexibility of nanometer-precise electron-beam lithography, thermal evaporation, and lift-off processing on 100-nm-thick silicon nitride membranes transparent for soft x rays. The disks have a diameter of 2 μm. The center-to-center distances of the disks are 2.25 μm and 3 μm, respectively, for two different sample types. Measurements are performed at the MAXYMUS beamline at BESSY II in Berlin, Germany. At first the whole crystal is strongly excited by an alternating unidirectional magnetic field that causes all the vortices to permanently switch their polarizations. The field amplitude is then reduced quasistatically (millisecond time scale) with respect to the periodicity of the vortex gyration (nanosecond time scale). As depicted in the inset of Fig. 1(a), starting from above the switching threshold, the amplitude of the harmonic excitation is reduced until switching dies out. In a second step,

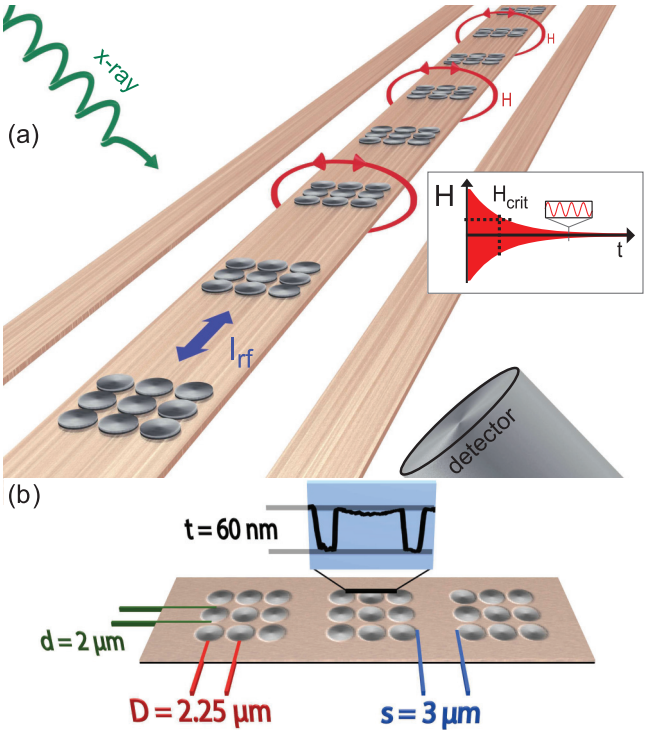

FIG. 1. (Color online) Experimental setup. (a) Vortex arrays investigated with transmission soft-x-ray microscopy. The magnetic field H is applied via an alternating current send through a coplanar waveguide. Inset: The amplitude of the unidirectional harmonic excitation is reduced until vortex-core switching ceases. (b) X-ray micrograph with in-plane contrast of three vortex arrays that comprise nine nanodisks each. The magnetization curls in plane around the center of each disk (thickness $t = 60$ nm, diameter $d = 2$ μm, and distance $D = 2.25$ μm). The inset shows a line scan of an atomic force micrograph and reveals the topography of the disks.

the patterns are determined by evaluating the sense of gyration of the vortices (see Supplemental Material,[25] movie 1). For this, a harmonic field of decreased amplitude is applied to noninvasively detect the created polarization pattern. For the determination of the polarization patterns, e.g., for 245 MHz, a time period of 4.08 ns is detected in steps of 80 ps. We find the vortices organized in preferred polarization states depending on the frequency of the excitation.

Since the process of switching itself cannot be investigated in the experiment, additional micromagnetic simulations have been performed. Those reveal that the vortex polarizations in an array of disks switch rather randomly at high amplitudes of a harmonic field that is applied to all magnetic vortices in the array. At intermediate field amplitudes the switching stops when certain stable polarization configurations are reached eventually. Movie 2 in the Supplemental Material[25] shows the pattern generation of a 3×3 crystal exposed to such an alternating field of constant harmonic amplitude ($\mu_0 H = 3$ mT). Note that the adiabatic field reduction in the experiments ensures that a suitable field amplitude where certain polarization configurations are stable is applied for a sufficiently large number of gyration periods.

The magnetic vortices couple in the manner of harmonic oscillators, whereas the coupling strength depends on the

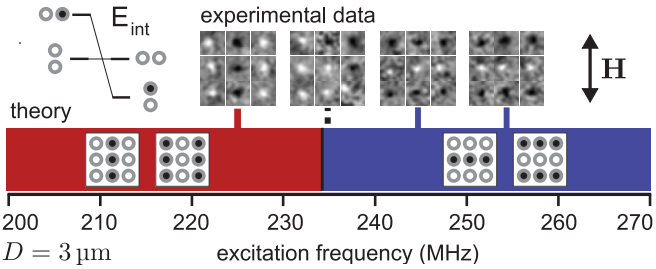

FIG. 2. (Color online) Theoretical prediction for stable vortex-core polarization states along with experimentally determined patterns. The predicted states are color coded. The four 3×3 arrays of square micrographs (190×190 nm^2) show Gaussian-filtered snapshots of the movies captured by transmission x-ray microscopy. The vortex cores appear as white or black dots according to their up- or downward polarization. At low (high) excitation frequencies a pattern of alternating vertical columns (horizontal rows) of constant polarization is predicted. The sketch in the upper left illustrates the interaction energies for different pairs of interacting vortices in the dipole model. The position of separation of the two patterns is calculated in the coupled Thiele model.

distance between the magnetic nanodisks containing the vortex cores.[26–29] When the center-to-center distance between the disks exceeds twice the diameter, the coupling can be neglected.[30,31] Random polarization patterns should emerge, independent of the excitation amplitude. Maximal coupling can be obtained by reducing the center-to-center distance between the disks until it equals the disk radius and the disks merge into a single structure. Smaller distances lead to exchange interaction at the intersection of the disks and will not be regarded here.[14] We experimentally investigate two types of samples of spatially separated disks with different center-to-center distances. The disk arrays of type 1 have a center-to-center distance of 3 μm, i.e., 1.5 times the diameter. For samples of type 2 the center-to-center distance of the disks is reduced to 2.25 μm (1.125 times the diameter) so as to obtain a strong dipolar coupling.[27,30]

For samples of type 1 the polarization alternates along the field direction and is constant in the perpendicular direction for excitation frequencies that are above 235 MHz. Rows of constant polarization occur. In contrast, columns of constant polarization occur at a frequency that is below 235 MHz. When excited at 235 MHz no pattern could reproducibly be tuned for repeated measurements on the same crystal. Figure 2 summarizes these experimental results performed at four different frequencies. The crystals show a large disk interdistance of 3 μm so that the coupling can be considered weak.[30,31] In the weak-coupling regime, the vortices behave almost like isolated vortices and the state formation can be understood in a fundamental model that is based on the coupling between two rotating magnetic dipoles. Viewed from far away, the in-plane stray field of a gyrating magnetic vortex resembles the stray field of a rotating magnetic dipole.[30] For an isolated vortex excited with a harmonic unidirectional field that points in the y direction, the sense of rotation of the dipole $\vec{p}_i$ depends only on the polarization $p_i \in \{-1,1\}$ of the magnetic vortex i,

$$\vec{p}_i \propto (-p_i \sin(\omega t + \varphi), \cos(\omega t + \varphi), 0)^T. \qquad (1)$$

The dipole field does not depend on the chirality. The inversion of the sign of the dipole by changing the chirality of the vortex is canceled out by a phase shift of 180° of the excited vortex gyration. A 3 × 3 vortex crystal may be formed from pairs of horizontally and vertically coupling vortices as building blocks. For the following comparison the interaction energy of two dipoles of varying polarities p_i and p_j,

$$E_{\mathrm{int},ij} = \frac{\mu_0}{8\pi} \int dV_i \int dV_j \frac{\varrho_i \varrho_j}{\|\vec{r}_i - \vec{r}_j\|}, \tag{2}$$

is integrated over one period of gyration $2\pi\omega^{-1}$. Here $\varrho_i = \vec{p}_i \vec{\nabla} \delta(\vec{r}_i - \vec{T}_i)$ denotes the charge distribution of the point dipoles. The vectors $\vec{T}_i$ point to the centers of the magnetic disks. The interaction energy splits, depending on the orientation of the disks with respect to the direction of the exciting field. Two cases are regarded: In the first case the interconnecting vector $\vec{D} = \vec{T}_1 - \vec{T}_2$ of the two dipoles points parallel to the field excitation, whereas it points perpendicular to the field excitation for the second case. When the pair of disks of alternating polarization $p_1 p_2 = -1$ is placed parallel to the direction of the excitation field the interaction energy is lower than for the same pair arranged perpendicular to the field excitation. For disks of identical polarization $p_1 p_2 = 1$ the interaction energy is identical for both orientations and lies in between the split energies of the alternating-polarization cases (see the sketch in Fig. 2). The energy splitting is correlated with the resonance frequency of the excited configuration. Low interaction energy reduces the resonance frequency of the system with respect to a system with higher interaction energy. A resonant excitation leads to switching at low excitation amplitudes and thereby to instability of the polarization pattern. When strongly excited, the system will settle in its most stable state. Thus, a pair of coupled vortices aligned parallel to the field excitation is stable at high frequencies for alternating polarizations and at low frequencies for identical polarizations, respectively. For a pair of coupled vortices aligned perpendicular to the field excitation this relation inverses. It is stable at low (high) frequencies for $p_1 p_2 = -1$ ($p_1 p_2 = 1$). The emergence of stable patterns can be explained by the combination of such differently aligned pairs. For high frequencies rows of constant polarization form, because pairs of identical polarizations are stable perpendicular to the field excitation. Within one column alternating polarizations occur since pairs of alternating polarizations are stable parallel to the field excitation. Consequently, columns of constant polarization and rows of alternating polarizations are predicted at low frequencies.

The dipole model accounts for the weak-coupling regime and motivates the experimentally observed state formation in the measurements presented above. When the interdisk distance is reduced, the coupling is increased and affects the relative motion of the vortices. Thus, the simple dipole model cannot be applied. We investigate this strong-coupling regime in an equivalent experiment with the vortex crystals of type 2 that have a smaller interdisk space of only 0.25 μm. As depicted in Fig. 3, we observe different polarization patterns for five excitation frequencies between 225 and 260 MHz. To elucidate the observation of the different patterns we use a theoretical model where the coupling between the vortices is modeled by surface charges that emerge when the vortex is

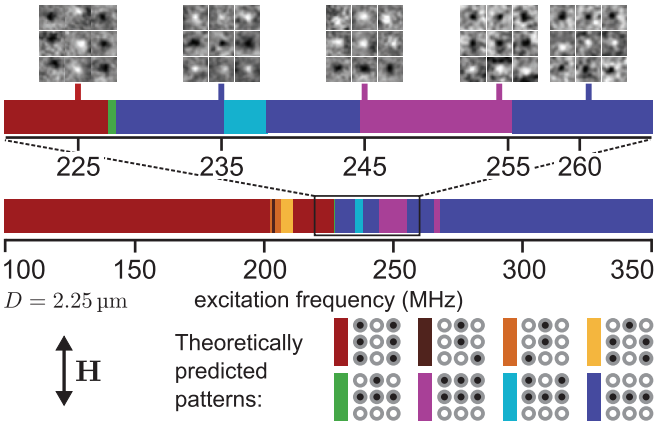

FIG. 3. (Color online) Theoretical prediction for stable vortex-core polarization states along with experimentally determined patterns. The predicted states are color coded. The five 3 × 3 arrays of square micrographs (190 × 190 nm^2) show Gaussian filtered snapshots of the movies captured by transmission x-ray microscopy. The vortex cores appear as white or black dots according to their up- or downward polarization. In the top graph the experimental frequency range is depicted in detail. When patterns are equivalent due to symmetry reasons only one representative pattern is shown. The limiting case at low (high) excitation frequencies [dark red (dark blue)] exhibits a vertical column (horizontal row) pattern. The frequency of the gyrotropic mode of an isolated vortex f = 238 MHz. [For further model parameters see the Supplemental Material (Ref. 25).]

deflected from the center of its disk.[20,26] The model is based on the analytical Thiele-Model[32] that allows describing the dynamics of a vortex as a quasiparticle.[33] The minimization of all micromagnetic energies E is expressed by a force $\vec{F} = -\vec{\nabla} E$ with energy contributions adapted to the geometry containing the magnetic vortex. The exchange and demagnetization energy is modeled by a two-dimensional harmonic potential E_{harm}.[33] A Zeeman term $E_{\mathrm{Zee}}(t)$ takes external magnetic fields into account.[34] We analyze a system consisting of multiple interacting vortices. Thus, the particle model has to consider magnetostatic interaction of separated vortex structures. In the rigid-vortex model, surface charges emerge at the disk edges, leading to the conservation of magnetic induction. These surface charges substitute for the charge distribution of dipoles in Eq. (2). For small deflections $|\vec{A}| \ll R$ the energy $E_{\mathrm{int},ij}$ of the interacting surface charges of two vortices i and j can be written as

$$E_{\mathrm{int},ij} = C_i C_j \, (s \, \hat{\eta}_{ij} \cdot \vec{A}_j) \cdot \vec{A}_i. \tag{3}$$

The chiralities of the vortices are denoted by C_i and C_j. In addition, the interaction energy depends only on the deflection $\vec{A}_i$ of the vortices within the disks and the matrix $\hat{\eta}_{ij}$ of numerical integrals that contain the geometry, the magnetic properties, and the relative position of the coupled vortices (see the Supplemental Material[25] Sec. B). The scaling factor $s < 1$ takes into account the theoretically predicted and experimentally observed fact that the coupling strength is overestimated by the rigid-vortex approach.[29,35,36] According to the Maxwell superposition principle the interaction energy of multiple

interacting vortices is calculated by the sum of all pair interaction terms. Thus, in this model a single vortex is subjected to a force $\vec{F}_i$ of the form $\vec{F}_i = -\vec{\nabla} E_{\mathrm{harm},i} - \vec{\nabla} E_{\mathrm{Zee},i} - \vec{\nabla} \sum_{j \neq i} E_{\mathrm{int},ij}$. This model does not implement the polarization switching itself. Instead of switching their polarities the vortices settle at stationary orbits regardless of an overcritical field excitation. Nevertheless, we motivate the emergence of the polarization patterns by analysis of the stationary dynamics in the crystal: Due to coupling, the crystal has different eigenmodes depending on its polarization pattern. When an eigenmode is resonantly excited (at the correct frequency) the vortices in the crystal reach high velocities and are likely to switch their polarizations. The switching yields a new polarization pattern. Thus, a pattern can be considered rather stable at an excitation frequency when no eigenmode of the pattern can efficiently be excited. Consequently, the stationary velocities of the vortices are low. In this way the most stable pattern can be identified. We calculate numerically the mean squared velocities (absorption[37]) of the nine vortices in the crystal for all 512 possible polarization patterns. The configuration with the lowest mean squared velocity is considered to require the highest field amplitude to switch its polarization pattern and is thus the most stable one. Due to the symmetry of the arrays and the unidirectional excitation field some of the possible 512 states are equivalent in the coupled Thiele model. An in-plane rotation of the crystal of 180° or looking at the crystal from the other side of the stripline does not change the relative velocities. In particular, the two patterns measured at 245 and 255 MHz (see Fig. 3) are equivalent in the coupled Thiele model. For symmetry reasons, 136 nondegenerate states of different stability exist. Figure 3 shows the most stable states, calculated in the coupled Thiele model, in dependence on the excitation frequency. For very low and very high frequencies again alternating columns and alternating rows of constant polarization are predicted, respectively, concordant with the weakly coupled dipole model. At intermediate frequencies near the resonance frequency of an isolated disk several patterns occur on slightly changing the excitation frequency. The experimentally investigated frequencies lie in this intermediate band which is depicted in detail in the frequency band in the upper part of Fig. 3 (220–265 MHz). The theoretical prediction is in perfect agreement with the experiment. All of the five measurements show states that are predicted at the correct frequencies. We want to point out that the measured behavior is very reproducible. The measurement at 225 MHz has been performed for five additional crystals of the same geometry (see the Supplemental Material[25] Sec. C), always yielding the same polarization pattern of columns of constant polarization. The pattern that emerges at 245 MHz could be confirmed for three of four further crystals. Only one crystal showed a pattern of homogeneous polarization which is the second most stable pattern near this frequency. At a frequency of 235 MHz two additional crystals yield the patterns neighboring the predicted patterns (colored yellow and cyan in Fig. 3). These slight deviations from the theory might be due to imperfections in the preparation process. Measurements of several isolated vortices of the same preparation process revealed that the resonance frequency of the vortices deviates about ±10 MHz from disk to disk. Despite this, the behavior of the system seems to be very robust against these variations. Always the most stable or at least a state with a very high stability (e.g., the secondmost stable state) occurred at the particular frequency. In addition the coupled Thiele model can account for the strong- and the weak-coupling regimes. As predicted by the model of two locally coupled dipoles, rows and columns of constant polarization occur at high and low frequencies, respectively. According to the Thiele model the transition between the two patterns of the weak-coupling case (see Fig. 2) lies at 235 MHz. This presumably explains the difficulties in measuring reproducibly the pattern at 235 MHz for the weak-coupling case. The emerging patterns can be predicted by a fundamental stability criterion, in spite of the complexity of the investigated system, which has 512 possible states and numerous state transitions. The criterion is based on simple models that assume small excitations of the vortices within the disks and, most notably, do not implement the polarization switching itself. Nevertheless it is possible to correctly predict the emerging polarization states by energy minimization considerations.

We have demonstrated that ordered polarization patterns can be obtained via self-organization in magnonic vortex crystals. An adiabatic reduction of a high-frequency magnetic field excitation leads to a self-organized relaxation of the system into well-ordered states. The emerging states are the least efficiently excitable states at the corresponding frequency. Our work allows further research studies to tailor the characteristic properties of magnonic vortex crystals by tuning the polarization state. For example, the predominant direction of signal transfer through the vortex crystal can be tailored perpendicular to the columns or rows of constant polarization.[27] It is also predicted that the allowed energy bands in such a crystal can be adjusted via manipulation of the polarization pattern.[11]

We thank Ulrich Merkt and Benjamin Krüger for fruitful discussions and Michael Volkmann for superb technical assistance. We acknowledge the support of the Max Plank Institute for Intelligent Systems (formerly MPI for Metals Research), Department Schütz, and the MAXYMUS team, particularly Michael Bechtel and Eberhard Goering. Financial support of the Deutsche Forschungsgemeinschaft via the Sonderforschungsbereich 668 and the Graduiertenkolleg 1286 is gratefully acknowledged. This work has been supported by the excellence cluster "The Hamburg Centre for Ultrafast Imaging—Structure, Dynamics, and Centre of Matter at the Atomic Scale" of the Deutsche Forschungsgemeinschaft.

*cadolff@physnet.uni-hamburg.de

[1]N. Liu, H. Guo, L. Fu, S. Kaiser, H. Schweizer, and H. Giessen, Nat. Mater. **7**, 31 (2008).

[2]R. F. Wang, C. Nisoli, R. S. Freitas, J. Li, W. McConville, B. J. Cooley, M. S. Lund, N. Samarth, C. Leighton, V. H. Crespi, and P. Schiffer, Nature (London) **439**, 303 (2006).

[3]V. V. Kruglyak, S. O. Demokritov, and D. Grundler, J. Phys. D **43**, 260301 (2010).
[4]S. G. Gregory, K. F. Barlow, K. E. McLay, R. Kaul, D. Swarbreck, A. Dunham, C. E. Scott, K. L. Howe, K. Woodfine, C. C. A. Spencer, M. C. Jones, C. Gillson, S. Searle, Y. Zhou, F. Kokocinski, L. McDonald, R. Evans, K. Phillips, A. Atkinson, R. Cooper, C. Jones, R. E. Hall, T. D. Andrews, C. Lloyd, R. Ainscough, J. P. Almeida, K. D. Ambrose, F. Anderson, R. W. Andrew, R. I. S. Ashwell, K. Aubin, A. K. Babbage, C. L. Bagguley, J. Bailey, H. Beasley, G. Bethel, C. P. Bird, S. Bray-Allen, J. Y. Brown, A. J. Brown, D. Buckley, J. Burton, J. Bye, C. Carder, J. C. Chapman, S. Y. Clark, G. Clarke, C. Clee, V. Cobley, R. E. Collier, N. Corby, G. J. Coville, J. Davies, R. Deadman, M. Dunn, M. Earthrowl, A. G. Ellington, H. Errington, A. Frankish, J. Frankland, L. French, P. Garner, J. Garnett, L. Gay, M. R. J. Ghori, R. Gibson, L. M. Gilby, W. Gillett, R. J. Glithero, D. V. Grafham, C. Griffiths, S. Griffiths-Jones, R. Grocock, S. Hammond, E. S. I. Harrison, E. Hart, E. Haugen, P. D. Heath, S. Holmes, K. Holt, P. J. Howden, A. R. Hunt, S. E. Hunt, G. Hunter, J. Isherwood, R. James, C. Johnson, D. Johnson, A. Joy, M. Kay, J. K. Kershaw, M. Kibukawa, A. M. Kimberley, A. King, A. J. Knights, H. Lad, G. Laird, S. Lawlor, D. A. Leongamornlert, D. M. Lloyd, J. Loveland, J. Lovell, M. J. Lush, R. Lyne, S. Martin, M. Mashreghi-Mohammadi, L. Matthews, N. S. W. Matthews, S. McLaren, S. Milne, S. Mistry, M. J. F. Moore, T. Nickerson, C. N. O'Dell, K. Oliver, A. Palmeiri, S. A. Palmer, A. Parker, D. Patel, A. V. Pearce, A. I. Peck, S. Pelan, K. Phelps, B. J. Phillimore, R. Plumb, J. Rajan, C. Raymond, G. Rouse, C. Saenphimmachak, H. K. Sehra, E. Sheridan, R. Shownkeen, S. Sims, C. D. Skuce, M. Smith, C. Steward, S. Subramanian, N. Sycamore, A. Tracey, A. Tromans, Z. Van Helmond, M. Wall, J. M. Wallis, S. White, S. L. Whitehead, J. E. Wilkinson, D. L. Willey, H. Williams, L. Wilming, P. W. Wray, Z. Wu, A. Coulson, M. Vaudin, J. E. Sulston, R. Durbin, T. Hubbard, R. Wooster, I. Dunham, N. P. Carter, G. McVean, M. T. Ross, J. Harrow, M. V. Olson, S. Beck, J. Rogers, and D. R. Bentley, Nature (London) **441**, 315 (2006).
[5]A. K. Geim and K. S. Novoselov, Nat. Mater. **6**, 183 (2007).
[6]M. S. Dresselhaus, G. Dresselhaus, and R. Saito, Carbon **33**, 883 (1995).
[7]B. Lenk, H. Ulrichs, F. Garbs, and M. Münzenberg, Phys. Rep. **507**, 107 (2011).
[8]S.-K. Kim, J. Phys. D **43**, 264004 (2010).
[9]T. Shinjo, T. Okuno, R. Hassdorf, K. Shigeto, and T. Ono, Science **289**, 930 (2000).
[10]A. Wachowiak, J. Wiebe, M. Bode, O. Pietzsch, M. Morgenstern, and R. Wiesendanger, Science **298**, 577 (2002).
[11]J. Shibata and Y. Otani, Phys. Rev. B **70**, 012404 (2004).
[12]A. Barman, S. Barman, T. Kimura, Y. Fukuma, and Y. Otani, J. Phys. D **43**, 422001 (2010).
[13]Y. Liu, Z. Hou, S. Gliga, and R. Hertel, Phys. Rev. B **79**, 104435 (2009).
[14]S. Jain, V. Novosad, F. Y. Fradin, J. E. Pearson, V. Tiberkevich, A. N. Slavin, and S. D. Bader, Nat. Commun. **3**, 1330 (2012).
[15]Spatial resolution, 25 nm; maximum temporal resolution, 40 ps.
[16]B. Riccò, G. Torelli, M. Lanzoni, A. Manstretta, H. Maes, D. Montanari, and A. Modelli, Proc. IEEE **86**, 2399 (1998).
[17]B. Pigeau, G. de Loubens, O. Klein, A. Riegler, F. Lochner, G. Schmidt, L. W. Molenkamp, V. S. Tiberkevich, and A. N. Slavin, Appl. Phys. Lett. **96**, 132506 (2010).
[18]Micromagnum, http://micromagnum.informatik.uni-hamburg.de/.
[19]S.-B. Choe, Y. Acremann, A. Scholl, A. Bauer, A. Doran, J. Stöhr, and H. A. Padmore, Science **304**, 420 (2004).
[20]K. Y. Guslienko, B. A. Ivanov, V. Novosad, Y. Otani, H. Shima, and K. Fukamichi, J. Appl. Phys. **91**, 8037 (2002).
[21]B. Van Waeyenberge, A. Puzic, H. Stoll, K. W. Chou, T. Tyliszczak, R. Hertel, M. Fähnle, H. Brückl, K. Rott, G. Reiss, I. Neudecker, D. Weiss, C. H. Back, and G. Schütz, Nature (London) **444**, 461 (2006).
[22]T. Kamionka, M. Martens, A. Drews, B. Krüger, O. Albrecht, and G. Meier, Phys. Rev. B **83**, 224424 (2011).
[23]V. Novosad, M. Grimsditch, K. Y. Guslienko, P. Vavassori, Y. Otani, and S. D. Bader, Phys. Rev. B **66**, 052407 (2002).
[24]M. Martens, T. Kamionka, M. Weigand, H. Stoll, T. Tyliszczak, and G. Meier, Phys. Rev. B **87**, 054426 (2013).
[25]See Supplemental Material at http://link.aps.org/supplemental/10.1103/PhysRevB.88.224425 for movies, a detailed description of the Thiele model, and additional experimental results.
[26]J. Shibata, K. Shigeto, and Y. Otani, Phys. Rev. B **67**, 224404 (2003).
[27]A. Vogel, M. Martens, M. Weigand, and G. Meier, Appl. Phys. Lett **99**, 042506 (2011).
[28]H. Jung, K.-S. Lee, D.-E. Jeong, Y.-S. Choi, Y.-S. Yu, D.-S. Han, A. Vogel, L. Bocklage, G. Meier, M.-Y. Im, P. Fischer, and S.-K. Kim, Sci. Rep. **1**, 59 (2011).
[29]S. Sugimoto, Y. Fukuma, S. Kasai, T. Kimura, A. Barman, and Y. C. Otani, Phys. Rev. Lett. **106**, 197203 (2011).
[30]A. Vogel, A. Drews, T. Kamionka, M. Bolte, and G. Meier, Phys. Rev. Lett. **105**, 037201 (2010).
[31]J. Mejía-López, D. Altbir, A. H. Romero, X. Batlle, I. V. Roshchin, C.-P. Li, and I. K. Schuller, J. Appl. Phys. **100**, 104319 (2006).
[32]A. A. Thiele, Phys. Rev. Lett. **30**, 230 (1973).
[33]B. Krüger, A. Drews, M. Bolte, U. Merkt, D. Pfannkuche, and G. Meier, Phys. Rev. B **76**, 224426 (2007).
[34]B. Krüger, A. Drews, M. Bolte, U. Merkt, D. Pfannkuche, and G. Meier, J. Appl. Phys. **103**, 07A501 (2008).
[35]A. Vogel, A. Drews, M. Weigand, and G. Meier, AIP Adv. **2**, 042180 (2012).
[36]O. V. Sukhostavets, J. González, and K. Y. Guslienko, Phys. Rev. B **87**, 094402 (2013).
[37]A. Drews, B. Krüger, G. Selke, T. Kamionka, A. Vogel, M. Martens, U. Merkt, D. Möller, and G. Meier, Phys. Rev. B **85**, 144417 (2012).